First-principles investigation of ferroelectricity in perovskite compounds

R. D. King-Smith* and David Vanderbilt
Department of Physics and Astronomy, Rutgers University, Piscataway, New Jersey 08855-0849
(Received 16 August 1993)

We have used a first-principles ultra-soft-pseudopotential method in conjunction with an efficient preconditioned conjugate-gradient scheme to investigate the properties of a series of eight cubic perovskite compounds. The materials considered in this study are $BaTiO_3$, $SrTiO_3$, $CaTiO_3$, $KNbO_3$, $NaNbO_3$, $PbTiO_3$, $PbZrO_3$, and $BaZrO_3$. We computed the total-energy surface for zone-center distortions correct to fourth order in the soft-mode displacement, including renormalizations due to strain coupling. Quantities calculated for each material include lattice constants, elastic constants, zone-center phonon frequencies, Grüneisen parameters, and band structures. Our calculations correctly predict the symmetry of the ground-state structures of all compounds whose observed low-temperature structure retains a primitive five-atom unit cell. The database of results we have generated shows a number of trends which can be understood using simple chemical ideas based on the sizes of ions, and the frustration inherent in the cubic perovskite structure.

I. INTRODUCTION

The perovskites are an extremely important class of ferroelectric materials.[1] Generically these compounds have a chemical formula ABO_3 where A is a monovalent or divalent cation and B is a penta- or tetravalent metal. The perfect perovskite structure is very simple and has full cubic symmetry. It can be thought of as a lattice of corner sharing oxygen octahedra with interpenetrating simple cubic lattices of A and B cations. The B cations sit at the center of each oxygen octahedra while the A metal ions lie in 12-fold coordinated sites between the octahedra. The fascinating feature of the perovskite structure is the extreme ease with which it will undergo structural phase transitions; experimentally the perovskites exhibit a diverse range of phases including transitions to both ferroelectric and antiferroelectric states as well as structural transitions to states involving tilting of the oxygen octahedra.

In spite of the fact that the perovskites have been the subject of intense investigation since the discovery of ferroelectricity in barium titanate in the 1940s, there is still no complete understanding of the nature of the transitions in these materials. For example, given the chemical formula of a perovskite material, there are no reliable methods for predicting transition temperatures, whether a transition is first or second order, or even which phonons in the material will be responsible for transitions. In principle these quantities can be obtained by calculating the partition function given the ion-ion Hamiltonian of the crystal.[1] It is well established that both harmonic and anharmonic phonon-phonon couplings as well as phonon-strain couplings are essential ingredients for a description of the transitions observed in the perovskites. However, there is little quantitative knowledge about the interaction parameters of this Hamiltonian and an accurate determination of these variables is a challenging theoretical problem.

First-principles density functional calculations offer an attractive approach for enhancing our microscopic understanding of perovskites and other ferroelectrics. One of the earliest successes of this method was due to Rabe and Joannopoulos who combined conventional pseudopotential methods with renormalization-group theory to calculate the transition temperature of the narrow-band semiconductor GeTe.[2]

More recently there has been a flurry of activity to apply these methods to perovskite compounds. Cohen and Krakauer[3] used the all-electron full-potential linearized augmented-plane-wave (FLAPW) method to study ferroelectricity in $BaTiO_3$ within the local density approximation (LDA). They performed a series of frozen phonon calculations and demonstrated that the phase with full cubic symmetry is unstable with respect to zone-center distortions, in accord with the experimentally observed ferroelectric transition in this material. They went on to study the depth and shapes of the energy well with respect to soft-mode displacement, and to demonstrate that strain strongly influences the form of the total-energy surface. Later they extended this approach to the case of $PbTiO_3$.[4] Using experimental data as a guide they were able to show that the observed tetragonal ferroelectric ground state of this material is stabilized by the large strain which appears upon transition from the cubic structure. Cohen emphasized that the hybridization between the titanium $3d$ and oxygen $2p$ is necessary for ferroelectricity in $BaTiO_3$ and $PbTiO_3$.[5] Singh and Boyer have also used the FLAPW method to investigate ferroelectricity in $KNbO_3$.[6] They found that the cubic structure was stable at the theoretical lattice constant, at variance with experimental observations, although their calculations did show weak ferroelectric behavior when they set the lattice constant to the experimental value. The FLAPW studies have demonstrated that ferroelectricity in the perovskites reflects a delicate balance between long-range electrostatic forces which favor the ferroelectric state and short-range repulsions which favor the cubic phase. Thus it has been demonstrated that

high-quality LDA calculations can shed considerable insight into the nature of the total-energy surface in the perovskites. However, the work also raises a note of caution about the validity of the LDA. For example the work of Singh and Boyer[6] suggests that $KNbO_3$ is not a ferroelectric in this approximation.

Recently we have applied the ultrasoft-pseudopotential method to investigate ferroelectricity in $BaTiO_3$.[7] Pseudopotential methods offer a number of advantages over all-electron methods. They are computationally more efficient than methods such as the FLAPW, and moreover allow one to compute forces on the ions analytically. Methods which provide information on Hellmann-Feynman forces allow the adiabatic energy surface to be explored with many fewer calculations than techniques which only compute total energies. However, the use of a pseudopotential does introduce further approximations beyond the LDA, associated with neglect of the core states and other transferability issues. The results of our calculation on $BaTiO_3$,[7] which included Ba and Ti semicore states, were in substantial agreement with the work of Cohen and Krakauer. We thus demonstrated that this approach can attain the level of accuracy necessary to capture the physics of the of ferroelectricity in the perovskites.

In the present paper we have chosen to apply the ultrasoft-pseudopotential approach to a series of eight perovskites, thus greatly increasing the amount of first-principles data available on these materials. Again, we include semicore states in the valence shell for all metals considered. The compounds selected for study were $BaTiO_3$, $SrTiO_3$, $CaTiO_3$, $KNbO_3$, $NaNbO_3$, $PbTiO_3$, $PbZrO_3$, and $BaZrO_3$. The properties of these materials are reviewed in Refs. 1 and 8. Experimentally all of these compounds are observed to have the perfect cubic perovskite structure at sufficiently high temperatures. Three of these materials, $BaTiO_3$, $KNbO_3$, and $PbTiO_3$, are observed to have ferroelectric ground states with five atoms in the primitive cell. Both $BaTiO_3$ and $KNbO_3$ are observed to undergo the same sequence of transitions as a function of temperature from the perfect cubic perovskite structure, to a tetragonal phase, to an orthorhombic phase before becoming rhombohedral at the lowest temperatures. By way of contrast $PbTiO_3$ has a single well-established transition from the cubic to the tetragonal phase at 493 °C. $SrTiO_3$ is an incipient ferroelectric which undergoes a nonferroelectric oxygen tilting transition at about 105 K. $CaTiO_3$ undergoes a single transition from the cubic state to an orthorhombic phase with 20 atoms in the unit cell at about 1260 °C. $NaNbO_3$ shows at least six transitions as a function of temperature. Its ground state is a monoclinic ferroelectric phase with four formula units per unit cell. $PbZrO_3$ is an antiferroelectric compound with eight formula units per unit cell. The transition from the cubic phase occurs at about 230 °C. Finally $BaZrO_3$ is the simplest material considered here and is believed to have the perfect cubic perovskite structure at all temperatures.

Our approach has been to focus exclusively on the possible zone-center instabilities of these materials. This restriction has a number of important practical advantages. First, as will be demonstrated in the following sections, the number of degrees of freedom of the system in this case is small enough to allow us to perform a completely systematic expansion of the energy to fourth order in the soft-mode displacement vector, without the need for experimental input which might bias our results. Second, this simplification allows us to focus on trends in the total-energy surface with composition even when the experimental situation may be much more complicated. For example it is clear from the previous discussion that the experimental behavior of each compound in the $BaTiO_3$, $SrTiO_3$, $CaTiO_3$ series is quite different. By concentrating on the relatively small number of parameters associated with zone-center distortions we might hope to begin to unravel the origins of these differences in these chemically similar materials. Finally, by choosing to work with the smallest possible cells we can afford to use very high-quality k-point sets for the Brillouin zone integrations. In the following it will be demonstrated that it is important to ensure that calculations are exceptionally well converged in this respect when studying ferroelectricity in the perovskites.

The remainder of this paper is set out as follows. In Sec. II we develop our systematic expansion of the soft-mode total-energy surface about the cubic perovskite structure. Section III describes some of the technical aspects of our work and discusses the convergence of our calculations. We present the results of our calculations in Sec. IV, and comment on some of the implications of the results in Sec. V. We review the main conclusions of this study in Sec. VI. Appendix A contains some of the more formal parts of the derivation of the energy expansion about the cubic perovskite structure. Appendix B describes our conjugate-gradient technique for minimizing the Kohn-Sham energy functional. Unless otherwise stated all results in the following sections are quoted in atomic units (i.e., lengths in bohrs and energies in hartrees).

II. FORMALISM

In order to carry out our investigation of the total-energy surfaces of the eight compounds in question it will be useful to develop a systematic expansion for the energy about the cubic perovskite structure. Our goal is to compute the minimum energy of configuration of the ions in the structure. It is well known that strain degrees of freedom play a significant role in determining the energies of the low-symmetry ferroelectric phases and should therefore be included in the analysis.[1,3,4] As stated in the Introduction we shall exclude from consideration any distortions which change the number of atoms in the unit cell. At first sight our task of performing a systematic exploration of the energy surface poses a formidable challenge, because even if we only include zone-center distortions and strains we are still faced with examining the properties of an 18-dimensional energy space.[4] However, we shall show that a manageable scheme for carrying through this program can be developed provided we restrict ourselves to computing the energy correct to fourth order in the soft-mode displacement. The high symme-

try of the cubic perovskite structure greatly reduces the number of calculations which are required. Our expansion of the energy is similar in spirit to that of Pytte,[9] although it differs in some details.

Formally the energy of the crystal is function of the six independent components of the strain tensor η_i, where i is a Voigt index ($\eta_1 = e_{11}, \eta_4 = 2e_{23}$), and the 15 displacement variables v_α^τ, where τ is an atom label and α is a Cartesian direction. Thus we may write the energy per unit cell as

$$E = E(\{\eta_i\}, \{v_\alpha^\tau\}). \tag{1}$$

In the following we shall make extensive use of the fact that

$$E(\{\eta_i\}, \{v_\alpha^\tau\}) = E(\{\eta_i\}, \{-v_\alpha^\tau\}). \tag{2}$$

Equation (2) follows by virtue of the fact that each atom in the perovskite structure sits at a center of inversion upon application of an arbitrary homogeneous strain. Formally it will be helpful to divide the energy function into parts arising from pure displacement, pure strain, and an interaction term as

$$E = E^0 + E^{\rm disp}(\{v_\alpha^\tau\}) + E^{\rm elas}(\{\eta_i\}) + E^{\rm int}(\{\eta_i\}, \{v_\alpha^\tau\}), \tag{3}$$

where E^0 is the energy of the perfect perovskite structure. $E^{\rm disp}(\{v_\alpha^\tau\})$ and $E^{\rm elas}(\{\eta_i\})$ give a description of the energy to all orders at zero strain and zero displacement respectively. In crystals with cubic symmetry the strain energy is given, correct to second order in the strains, by

$$\begin{aligned} E^{\rm elas}(\{\eta_i\}) = &\frac{1}{2}B_{11}(\eta_1^2 + \eta_2^2 + \eta_3^2) \\ &+ B_{12}(\eta_1\eta_2 + \eta_2\eta_3 + \eta_3\eta_1) \\ &+ \frac{1}{2}B_{44}(\eta_4^2 + \eta_5^2 + \eta_6^2), \end{aligned} \tag{4}$$

where B_{11}, B_{12}, and B_{44} are related by factors of the cell volume to the elastic constants of the crystal.

We begin by considering in detail the expansion of $E^{\rm disp}(\{v_\alpha^\tau\})$. Straightforward Taylor expansion of the energy implies that the lowest-order term can be written as $\frac{1}{2}\sum_{\tau,\tau',\alpha,\beta} D_{\alpha,\beta}^{\tau,\tau'} v_\alpha^\tau v_\beta^{\tau'}$ where $D_{\alpha,\beta}^{\tau,\tau'} = \left.\frac{\partial^2 E}{\partial v_\alpha^\tau \partial v_\beta^{\tau'}}\right|_0$. The second derivative matrix $D_{\alpha,\beta}^{\tau,\tau'}$ is of course related to the zone-center dynamical matrix by trivial factors of the ionic masses. The symmetry properties of $D_{\alpha,\beta}^{\tau,\tau'}$ have already been discussed in the context of first-principles calculations.[3,6] In the following we shall adopt a coordinate system such that the atoms in our general perovskite with formula ABO_3 in the perfect structure have positions A at (0,0,0)a, B at $(\frac{1}{2},\frac{1}{2},\frac{1}{2})a$, $O_{\rm I}$ at $(0,\frac{1}{2},\frac{1}{2})a$, $O_{\rm II}$ at $(\frac{1}{2},0,\frac{1}{2})a$, and $O_{\rm III}$ at $(\frac{1}{2},\frac{1}{2},0)a$, where a is the lattice constant. The first point to note is that all elements of $D_{\alpha,\beta}^{\tau,\tau'}$ for which $\alpha \neq \beta$ are zero (it is intuitive that displacement of any of the five sublattices in, say, the x direction will produce no forces in the y or z direction). The 15×15 second derivative matrix therefore breaks into a set of three independent and identical 5×5 blocks, each corresponding to displacements in the x, y, or z direction. As a consequence the eigenvalues of the second derivate matrix fall into five sets of threefold degenerate modes. In the following we will denote the eigenvalues of $D_{\alpha,\beta}^{\tau,\tau'}$ as $\lambda(j)$ where j is an index which runs from 1 to 5. Thus we may write

$$\sum_{\beta\tau'} D_{\alpha,\beta}^{\tau,\tau'} \xi_\beta^{\tau'}(j,\gamma) = \lambda(j)\xi_\alpha^\tau(j,\gamma). \tag{5}$$

Moreover, it is clear from the foregoing discussion that the eigenvectors, $\xi_\alpha^\tau(j,\beta)$, of the second derivative matrix can be chosen to lie entirely along x, y, or z and can thus be labeled by j and the Cartesian direction β. With this convention we will have $\xi_\alpha^\tau(j,\beta) = 0$ if $\alpha \neq \beta$. Two of the eigenvectors of each 5×5 block are determined by symmetry. The first mode is the trivial translation mode with eigenvalue 0. The second mode has Γ_{25} symmetry.[6] The eigenvector of this mode for displacements in the z direction has the form $(0,0,\frac{1}{\sqrt{2}},-\frac{1}{\sqrt{2}},0)$ where the displacement vector is listed in the order $(v_z^A, v_z^B, v_z^{O_{\rm I}}, v_z^{O_{\rm II}}, v_z^{O_{\rm III}})$. The remaining three modes of each block have Γ_{15} symmetry and their eigenvectors cannot be deduced on symmetry grounds alone. Experimentally it is these modes with Γ_{15} symmetry which are responsible for ferroelectric transitions from the high-symmetry cubic phase. In a material such as barium titanate where the experimental ground state is a five-atom unit cell with rhombohedral symmetry one expects at least one of the three Γ_{15} eigenvalues to have a negative sign, indicating that the cubic structure is a saddle point of the total-energy surface. In the following the lowest-frequency mode with Γ_{15} symmetry will be referred to as the *soft mode*.

We can reexpress $E^{\rm disp}$, correct to second order, in terms of the diagonalized $D_{\alpha,\beta}^{\tau,\tau'}$ matrix as

$$E^{\rm disp} = \frac{1}{2}\sum_j \lambda(j) \sum_\alpha u_\alpha^j u_\alpha^j, \tag{6a}$$

where u_α^j are eigenmode amplitudes given by

$$u_\alpha^j = \sum_\tau \xi_\alpha^\tau(j,\alpha) v_\alpha^\tau. \tag{6b}$$

Because of their special role in the following it will be convenient to introduce a simplified notation to describe the soft-mode distortions. If $j_{\rm soft}$ is the index of the soft mode, then we define

$$\kappa = \frac{1}{2}\lambda(j_{\rm soft}), \tag{7a}$$

and will suppress the j superscript for the soft-mode amplitude so that

$$u_\alpha = u_\alpha^{j_{\rm soft}}. \tag{7b}$$

Having decoupled the soft-mode degrees of freedom to second order in the displacements we now consider the effects of higher-order terms in the soft-mode expansion of the energy. We introduce $\Phi(\{u_\alpha\})$ which is $E^{\rm disp}$ with all

non-soft-mode eigenmode amplitudes held at zero. There can be no third-order terms in the displacement which contribute to $\Phi(\{u_\alpha\})$ by virtue of Eq. (2). Two independent parameters are required to describe the fourth-order terms and we find

$$\Phi(\{u_\alpha\}) = \kappa u^2 + \frac{1}{24}B_{xxxx}\sum_\alpha u_\alpha^4 + \frac{1}{4}B_{xxyy}(u_x^2u_y^2 + u_y^2u_z^2 + u_z^2u_x^2), \quad (8a)$$

where

$$B_{xxxx} = \left.\frac{\partial^4 E}{\partial u_x^4}\right|_0, \quad (8b)$$

$$B_{xxyy} = \left.\frac{\partial^4 E}{\partial u_x^2 \partial u_y^2}\right|_0, \quad (8c)$$

and $u^2 = \sum_\alpha u_\alpha^2$. It will simplify the notation if we introduce two new parameters α and γ defined by

$$\alpha = \frac{1}{24}B_{xxxx} \quad (9a)$$

and

$$\gamma = \frac{1}{12}(3B_{xxyy} - B_{xxxx}). \quad (9b)$$

Substituting into Eq. (8a) we obtain

$$\Phi(\{u_\alpha\}) = \kappa u^2 + \alpha u^4 + \gamma(u_x^2u_y^2 + u_y^2u_z^2 + u_z^2u_x^2). \quad (10)$$

The constant γ gives a measure of the anisotropy of the total-energy surface. In the following we shall be primarily concerned with the case where there are zone-center instabilities so that $\kappa < 0$. Under these circumstances it can be shown that Φ has four distinct types of stationary points. The first of these is the trivial case where $u_x = u_y = u_z = 0$, with $\Phi = 0$. This is always a maximum of Φ when $\kappa < 0$ indicating that the crystal is unstable in the cubic perovskite structure. There are six symmetry-equivalent stationary points of the second type. They lie along the $\langle 100\rangle$ directions and have positions such as

$$u_x = u_y = 0, \quad u_z = \sqrt{-\frac{\kappa}{2\alpha}}, \quad (11a)$$

with energy

$$\Phi = -\frac{\kappa^2}{4\alpha}. \quad (11b)$$

The third set of stationary points, of which there are 12, falls in the $\langle 110\rangle$ directions and has coordinates of the type

$$u_x = 0, \quad u_y = u_z = \sqrt{-\frac{\kappa}{4\alpha+\gamma}}, \quad (12a)$$

with energy

$$\Phi = -\frac{\kappa^2}{4(\alpha+\frac{1}{4}\gamma)}. \quad (12b)$$

Finally there are eight equivalent stationary points in the $\langle 111\rangle$ directions with positions such as

$$u_x = u_y = u_z = \sqrt{-\frac{\kappa}{6\alpha+2\gamma}}, \quad (13a)$$

with energy

$$\Phi = -\frac{\kappa^2}{4(\alpha+\frac{1}{3}\gamma)}. \quad (13b)$$

Necessary conditions for the above fourth-order analysis to be valid are that $\alpha > 0$ and $\gamma > -3\alpha$. Otherwise the energy has unphysical divergences to $-\infty$ implying that higher-order terms must be taken into account. Provided the fourth-order analysis is valid, two distinct ground states can arise depending on the sign of γ. If $\gamma > 0$, then Eq. (11b) is a global minimum and the crystal ground state has tetragonal symmetry. If $\gamma < 0$, then the global minima are along the $\langle 111\rangle$ directions and the ground state has rhombohedral symmetry with energy given in Eq. (13b).

Finally we must consider how the above picture is modified when we permit possible extra relaxations of the system through coupling of the soft modes to other phonons and the strains. The basic strategy is to compute the values of η_i and u_α^j which minimize the total energy as a function of the soft-mode variables. Following the notation of Ref. 10 we denote these minimizing values with $\tilde{\eta}_i(\{u_\alpha\})$ and $\tilde{u}_\alpha^j(\{u_\alpha\})$ and the corresponding energy with $\tilde{E}(\{u_\alpha\})$. By straightforward differentiation of Eq. (3) it can be shown that the only term which leads to renormalization of the soft-mode surface, in the fourth-order theory, is the lowest-order term in $E^{\rm int}$.[11] This term can be written in the form $\frac{1}{2}\sum_{i\alpha\beta}B_{i\alpha\beta}\eta_i u_\alpha u_\beta$, in an obvious notation. To second order in u_α, $\tilde{\eta}_i$ is given by the solution to the matrix equation

$$\sum_j B_{ij}\tilde{\eta}_i + \frac{1}{2}\sum_{\alpha\beta}B_{i\alpha\beta}u_\alpha u_\beta = 0. \quad (14)$$

There are three different types of nonzero elements in the $6\times3\times3$ matrix $B_{i\alpha\beta}$. Typical nonzero elements are B_{1xx}, B_{1yy}, and B_{4yz}. The renormalized energy is given by

$$\tilde{E}(\{u_\alpha\}) = E^0 + \Phi(\{u_\alpha\}) - \frac{1}{8}\sum_{ij}\sum_{\alpha\beta\gamma\delta}u_\alpha u_\beta B_{i\alpha\beta}N_{ij}B_{j\gamma\delta}u_\gamma u_\delta, \quad (15)$$

where $N_{ij} = [B^{-1}]_{ij}$. The solution of Eq. (14) to obtain $\tilde{E}(\{u_\alpha\})$ in Eq. (15) is somewhat tedious, and is therefore deferred to Appendix A. It is shown there that

$$\widetilde{E}(\{u_\alpha\}) = E^0 + \Phi(\{u_\alpha\}) - \frac{1}{24}\left(\frac{C^2}{B} + 4\frac{\nu_t^2}{\mu_t}\right)\sum_\alpha u_\alpha^4 - \frac{1}{12}\left(\frac{C^2}{B} - 2\frac{\nu_t^2}{\mu_t} + 6\frac{\nu_r^2}{\mu_r}\right)(u_x^2u_y^2 + u_y^2u_z^2 + u_z^2u_x^2), \tag{16}$$

where B is the bulk modulus,

$$B = B_{11} + 2B_{12}, \tag{17a}$$

μ_t and μ_r are shear moduli for tetragonal and rhombohedral distortions,

$$\mu_t = \frac{1}{2}(B_{11} - B_{12}), \tag{17b}$$

$$\mu_r = B_{44}, \tag{17c}$$

and C, ν_t, and ν_r are analogously defined quantities obtained from the strain-phonon coupling constants,

$$C = B_{1xx} + 2B_{1yy}, \tag{17d}$$

$$\nu_t = \frac{1}{2}(B_{1xx} - B_{1yy}), \tag{17e}$$

$$\nu_r = B_{4yz}. \tag{17f}$$

Comparing Eq. (16) with Eq. (8a) we arrive at the reassuring conclusion that the fourth-order corrections to the minimum energy $\widetilde{E}(\{u_\alpha\})$ arising from soft-mode coupling to the strain have exactly the same structure as the original "bare" fourth-order terms. The net effect of switching on the coupling between the phonon and strain degrees of freedom can be thought of as a renormalization of the bare fourth-order interaction coefficients B_{xxxx} and B_{xxyy} to B'_{xxxx} and B'_{xxyy} defined by

$$B'_{xxxx} = B_{xxxx} - \left(\frac{C^2}{B} + 4\frac{\nu_t^2}{\mu_t}\right) \tag{18a}$$

and

$$B'_{xxyy} = B_{xxyy} - \frac{1}{3}\left(\frac{C^2}{B} - 2\frac{\nu_t^2}{\mu_t} + 6\frac{\nu_r^2}{\mu_r}\right). \tag{18b}$$

We therefore conclude that our analysis of the stationary properties of the total-energy surface can equally well be applied to the case where phonon-strain couplings are present, provided we work with renormalized coupling constants α' and γ' where

$$\alpha' = \alpha - \frac{1}{24}\left(\frac{C^2}{B} + 4\frac{\nu_t^2}{\mu_t}\right) \tag{19a}$$

and

$$\gamma' = \gamma + \frac{1}{2}\left(\frac{\nu_t^2}{\mu_t} - \frac{\nu_r^2}{\mu_r}\right). \tag{19b}$$

Our final expression for $\widetilde{E}(\{u_\alpha\})$ is simply

$$\widetilde{E}(\{u_\alpha\}) = E^0 + \kappa u^2 + \alpha' u^4 + \gamma'(u_x^2u_y^2 + u_y^2u_z^2 + u_z^2u_x^2). \tag{20}$$

In the case where $\kappa < 0$ there are two possible ground states in the complete fourth-order theory. If $\gamma' < 0$, we would predict that a phase with rhombohedral symmetry has the lowest energy, where as $\gamma' > 0$ implies that the ground state is tetragonal. In the following section our objectives are to use high-quality first-principles calculations to obtain the various expansion parameters necessary to determine the constants in Eq. (20).

In conclusion we have shown that the minimum total energy as a function of soft-mode displacement can be determined correct to fourth order in u_α in terms of nine independent interaction parameters κ, B_{11}, B_{12}, B_{44}, B_{1xx}, B_{1yy}, B_{4yz}, B_{xxxx}, and B_{xxyy}. We have found that in practice these quantities can be computed using about 40 self-consistent calculations per material. The major formal results are that coupling of the soft mode to the strain renormalizes the minimum energy surface in our fourth-order approximation, whereas coupling to other phonons does not. The quadratic coefficient in the total energy, κ, is unrenormalized by either phonon or strain interactions.

III. TECHNICAL DETAILS OF CALCULATIONS

The first-principles calculations presented in this paper were performed using the Vanderbilt ultrasoft-pseudopotential scheme.[12] Technical details of this method and its implementation in solid-state calculations have already been discussed elsewhere.[7,13–16] A feature of the present work is the use of a conjugate-gradient technique for minimizing the Kohn-Sham energy functional, as described in Appendix B.

The ultrasoft-pseudopotential approach has two major advantages. First, it allows us to work with a modest plane-wave cutoff, despite the presense of both first-row atoms and first-row transition metal atoms, which are generally difficult cases for pseudopotential methods.[17] This is accomplished at the expense of introducing a generalized eigenvalue equation containing an overlap operator, and generalizing the usual definition of the valence charge density to include an augmentation step. The ultrasoft potentials are a little more complicated than the original Kleinman-Bylander separable potentials.[18] However, the computational costs associated with the extra steps in the calculations only add a small fraction to the time required per conjugate-gradient iteration.

Second, it allows for the generation of exceptionally transferable pseudopotentials, because of its use of multiple reference energies during the construction procedure.[12] In essence the scheme allows one to insist that the all-electron and pseudologarithmic derivatives agree at two or three energies, instead of at just one energy.[19] This ensures that the all-electron and pseudo-atom scattering properties agree over an exceptionally wide energy range. Moreover, it allows us to treat ex-

TABLE I. Transferability of the titanium pseudopotential. All-electron $3s$, $3p$, $4s$, and $3d$ eigenvalues are given in hartrees; Δ is the corresponding difference between the all-electron eigenvalue and pseudoeigenvalue, in mhartree. $\Delta = 0$ in the reference $3s^2 3p^6 4s^2 3d^1$ configuration by construction.

Configuration	$3s$	$\Delta(3s)$	$3p$	$\Delta(3p)$	$4s$	$\Delta(4s)$	$3d$	$\Delta(3d)$
$3s^2 3p^6 4s^2 3d^2$	-2.288023	-0.2	-1.425332	-0.3	-0.169049	0.0	-0.164012	0.2
$3s^2 3p^6 4s^2 3d^1$	-2.765159	0.0	-1.893377	0.0	-0.445220	0.0	-0.592621	0.0
$3s^2 3p^6 4s^2 3d^0$	-3.359884	0.5	-2.475773	0.3	-0.783472	0.0	-1.139811	-1.1
$3s^2 3p^6 4s^1 3d^1$	-3.104766	0.1	-2.231605	0.1	-0.707960	0.0	-0.921973	0.0
$3s^2 3p^6 4s^0 3d^0$	-4.175466	0.0	-3.285763	0.2	-1.359890	0.6	-1.930327	0.3
$3s^2 3p^5 4s^2 3d^1$	-3.396932	-1.8	-2.511765	-2.1	-0.790393	0.1	-1.169291	0.2

plicitly the "shallow" core states in the calculation by including multiple sets of occupied states in each angular momentum channel. This helps to improve the chemical hardness of the potential.[20] Moreover, there is evidence that explicit treatment of the semicore levels is necessary to correctly describe the phonon instabilities of perovskites and related materials.[21]

Semicore shells have been included in the present calculation for all the metals considered. Specifically, we include as valence states the $2s$ and $2p$ states of Na; the $3s$ and $3p$ states of K, Ca, and Ti; the $4s$ and $4p$ states of Sr, Zr, and Nb; and the $5s$ and $5p$ states of Ba. We also include the $5d$ shell in Pb. Thus, we have been much more conservative about our choice of what constitutes a valence state than is generally the case in the pseudopotential method.[22] This is motivated by the need for high accuracy when studying the ferroelectric instabilities in perovskites.

Other details are as follows. Relativity was included by first performing scalar relativistic calculations on all-electron atoms,[23] and then applying a suitable generalization of the pseudization procedure proposed by Kleinman.[24] The oxygen potential used two construction energies each in the s and p channels. The potentials for the metals in this study all employed two reference energies per angular momentum in s, p, and d channels. The pseudo-wave-functions were constructed using the optimized potential method proposed by Rappe *et al.*,[17] by minimizing the kinetic energy of the pseudo-wave-function above the plane-wave cutoff, which we chose to be 25 Ry throughout our calculations. A variant of the same scheme was also applied to generate pseudo-charge-augmentation functions. In this case the cutoff for the optimization step was chosen to be 100 Ry, because the cutoff energy for the potentials and densities in plane-wave methods is generally 4 times as large as that for the wave functions.

Our tests suggest that the potentials in this study are of very high quality. We shall consider in more detail the case of Ti, which is probably the least transferable of the ten pseudopotentials required for this study. There are two main tests of pseudopotential transferability in common use. The first involves checking that the logarithmic derivatives of the all-electron and pseudoatom agree over a reasonable range of energies. In a previous publication we showed that our titanium potential does an exceptional job of matching the all-electron logarithmic derivatives over a 4 hartree range of energy.[7] The second main test is to check that the all-electron atoms and pseudoatoms have similar eigenvalues when the ionization state of the atom is changed. In Table I we summarize the results of our tests on the titanium potential. The atom was generated in the $3s^2 3p^6 4s^2 3d^1$ configuration and so Δ, the difference between the all-electron eigenvalues and pseudoeigenvalues in mhartree, is zero by construction for all states in this case. The largest values of Δ of -2.1 mhartree occur when an electron is removed from the $3p$ level. However, given the depth of

TABLE II. Convergence of eigenvalues and eigenvectors of $D^{\tau\tau'}_{\alpha\beta}$ with k-point set in $PbTiO_3$. The lower eigenvalues, which are a measure of potential soft-mode instability, are remarkably sensitive to the k-point sampling; this may be indicative of delicate cancellations between competing contributions to the force constants. Subsequent calculations use the (6, 6, 6) mesh.

k points	Eigenvalues	Eigenvectors			
2 2 2	-0.00918	-0.8679	0.0246	0.3244	0.3244	0.1885
	0.15538	-0.0620	0.5993	0.1207	0.1207	-0.7795
	0.16851	-0.2119	0.6631	-0.4236	-0.4236	0.3955
4 4 4	-0.01824	-0.6400	-0.4376	0.4062	0.4062	0.2622
	0.05070	-0.6145	0.7801	-0.0285	-0.0285	-0.1096
	0.15338	-0.1168	0.0003	-0.3655	-0.3655	0.8479
6 6 6	-0.02584	-0.5729	-0.5146	0.4074	0.4074	0.2732
	0.04422	-0.6765	0.7312	0.0144	0.0144	-0.0843
	0.15250	-0.1183	0.0027	-0.3657	-0.3657	0.8476
8 8 8	-0.02720	-0.5644	-0.5237	0.4066	0.4066	0.2765
	0.04350	-0.6830	0.7250	0.0210	0.0210	-0.0826
	0.15264	-0.1187	0.0059	-0.3665	-0.3665	0.8468

TABLE III. Convergence of eigenvalues and eigenvectors of $D^{\tau\tau'}_{\alpha\beta}$ with energy cutoff in $PbTiO_3$. Results appear to be well converged at 25 Ry, which is used as the cutoff for subsequent calculations.

Cutoff (Ry)	Eigenvalues	Eigenvectors				
25	-0.02584	-0.5729	-0.5146	0.4074	0.4074	0.2732
	0.04422	-0.6765	0.7312	0.0144	0.0144	-0.0843
	0.15250	-0.1183	0.0027	-0.3657	-0.3657	0.8476
50	-0.02400	-0.5961	-0.4888	0.4087	0.4087	0.2674
	0.04493	-0.6576	0.7489	-0.0055	-0.0055	-0.0804
	0.15565	-0.1099	-0.0106	-0.3645	-0.3645	0.8497

this state it is extremely unlikely that it could be depleted by anything approaching a single electron in the ground state of a real solid. The more important data are therefore the rows connected with removal of the valence $4s$ and $3d$ electrons. Typically the values of Δ are less than 0.5 mhartree in this case. Overall the agreement between all-electron eigenvalues and pseudoeigenvalues appears to be comparable with that achieved by Teter's recent extended-norm and hardness-conserving (ENHC) potentials, which represent the state of the art in this respect in more conventional pseudopotential technology.[20]

The solid-state calculations throughout this work were performed using a (6,6,6) Monkhorst-Pack mesh,[25] i.e., 6^3 points in the full Brillouin zone. The unit cells used here had either cubic, tetragonal, or rhombohedral symmetry, which yielded 10, 18, and 28 k points in the irreducible wedge of the zone respectively. This represents a k-point set of quite exceptional quality given that the materials in question are all insulators. However, our tests indicate that this level of accuracy is necessary when computing the properties of the soft-mode total-energy surface. For example Table II shows how the Γ_{15} symmetry eigenvalues and eigenvectors of the $D^{\tau\tau'}_{\alpha\beta}$ matrix converge as a function of k-point set quality in $PbTiO_3$. The second derivative matrix was constructed using a frozen phonon approach. The soft-mode eigenvalues $\lambda(j_{\rm soft}) = 2\kappa$, computed with the (4,4,4) and (6,6,6) Monkhorst-Pack mesh, differ by about 30%. The analysis of the previous section shows that the well depths depend on κ^2. We would therefore conclude that well depths computed with the (4,4,4) and (6,6,6) Brillouin zone meshes would disagree by 50% if the anharmonic terms were unaffected. This unusual sensitivity may be indicative of delicate cancellations between competing contributions to the restoring forces for soft-mode distortions.

A plane-wave cutoff of 25 Ry was used throughout our calculations, consistent with the optimization value used in our construction procedure. We have also tested the convergence of the Γ_{15} eigenvalues and eigenvectors of the $D^{\tau\tau'}_{\alpha\beta}$ matrix with respect to energy cutoff. Results are summarized in Table III. We find that κ changed by about 7% on increasing the cutoff from 25 to 50 Ry. The higher-frequency $\lambda(j)$ are converged to about 2% at 25 Ry. It would therefore appear that the error due to incomplete convergence of the basis set is of similar size to the k-point sampling error. The exchange and correlation was calculated using the Ceperley-Alder form.[26]

We conclude that our calculations are fairly well converged with respect to k-point sets and plane-wave cutoff, although there is room for improvement in these areas. It should be borne in mind that many previous studies on the perovskite compounds have used the (4,4,4) rather than (6,6,6) Monkhorst-Pack meshes.[3–6] We think that this is potentially a significant source of error, particularly when it comes to computing the depths of the ferroelectric wells.

IV. RESULTS

A. Lattice constants of the perovskites

We computed the value of the lattice constant which minimizes the energy of the structure when the ions are held fixed in the perfect cubic perovskite structure. Our results, in atomic units, are summarized in Table IV. The values obtained are in excellent accord with those calculated with the FLAPW method, in those cases where calculations exist. The first-principles results are generally 1–2 % smaller than the experimental values. This magnitude and sign of error are typical of high-quality total-energy calculations, which tend to underestimate lattice constants as a consequence of the LDA. For comparison we have also computed values of the lattice constant using Shannon-Prewitt radii.[27] We consider the possibility that the lattice constant is determined either by interaction of the 12-fold coordinated A cation and oxygen (A-O), or by interaction of the 6-fold coordinated B cation and oxygen (B-O). The ionic radius approach clearly tends to overestimate the lattice constant. In their original paper Shannon and Prewitt[27] noted that their method tends to perform relatively poorly for perovskites and other high-symmetry structures. Nevertheless, many of the trends observable in Table IV can be understood in terms of this simple picture. For example both the theoretical and experimental lattice constants are seen to decrease with decreasing radius of the A cation in the $BaTiO_3$, $SrTiO_3$, $CaTiO_3$ series. In a similar way we also find that the lattice constant increases on replacing Ti with the larger Zr ion in both $BaTiO_3$ and $PbTiO_3$.

In the final column of Table IV we introduce a quantity, δ, which is a length that measures the extent of the frustration between the competing (A-O) and (B-O) interactions in the cubic perovskite lattice. We define δ to be the difference between the cubic lattice constants predicted by the Shannon-Prewitt radii assuming that (A-O) and (B-O) interactions are dominant. Thus a value of δ close to zero, as found in $BaZrO_3$ or $SrTiO_3$, im-

TABLE IV. Cubic perovskite lattice constants in bohrs.

Compound	This work	FLAPW	Experiment	(A-O)	(B-O)	δ
$BaTiO_3$	7.456	7.45[a]	7.58	8.02	7.58	0.44
$SrTiO_3$	7.303		7.38	7.59	7.58	-0.01
$CaTiO_3$	7.192		7.25	7.35	7.58	-0.23
$KNbO_3$	7.472	7.488[b]	7.58	8.02	7.71	0.31
$NaNbO_3$	7.396		7.44	?[e]	7.71	?[e]
$PbTiO_3$	7.350	7.35[c]	7.50	7.72	7.58	0.14
$PbZrO_3$	7.770		7.81[d]	7.72	8.01	-0.29
$BaZrO_3$	7.853		7.924	8.02	8.01	0.01

[a] Ref. 3.
[b] Ref. 6.
[c] R.E. Cohen (private communication).
[d] Calculated assuming the same density as the tetragonal phase.
[e] Value not calculated as tables do not include value for 12-fold coordinated Na^+.

plies that both A and B cations are simultaneously satisfied by their oxygen environment. The sign convention adopted here is such that a positive value of δ, as that found in $BaTiO_3$, implies that the hole for the B cation is stretched beyond its ideal value. In the following we shall explore the extent to which trends in the behavior of the perovskite compounds can be correlated with δ. The importance of competing (A-O) and (B-O) interactions in the perovskites has been emphasized previously and can be traced at least as far back as Slater's work on $BaTiO_3$.[28]

B. Zero-temperature structures of the perovskites in the LDA

Having obtained the lattice constant which minimizes the energy of the perfect cubic perovskite structure for each material, we went on to compute the soft-mode eigenvalues κ and eigenvectors introduced in Sec. II, using the frozen phonon method. Three calculations with different displacement patterns are sufficient to obtain the modes with Γ_{15} symmetry. We used displacements in the z direction of the form $(0.002,0,0,0,0)a$, $(0,0.002,0,0,0)a$, and $(0,0,0.001,0.001,-0.002)a$, where the displacement vector is listed in the order $(v_z^A, v_z^B, v_z^{O_I}, v_z^{O_{II}}, v_z^{O_{III}})$. Our results for κ are summarized in column 8 of Table V.

There are a number of interesting observations to be made about the values of κ obtained in this way. First, we find that κ is positive only for $BaZrO_3$. This result for $BaZrO_3$ is in accord with the experimental observation that this material is stable in the cubic perovskite structure at all temperatures. We would also expect the three compounds $BaTiO_3$, $KNbO_3$ and $PbTiO_3$, which have ferroelectric ground states with primitive five-atom unit cells, to have negative values of κ. This expectation is confirmed in Table V and Table VI where we summarize which compounds are theoretically ferroelectric, if we restrict attention to just the zone-center instabilities. Previous studies on $BaTiO_3$ (Refs. 3 and 7) and $PbTiO_3$ (Ref. 4) have found zone-center instabilities at the theoretical lattice constant. However, the previous LDA study on $KNbO_3$,[6] using the FLAPW method, found this material to be stable at the theoretical lattice constant, although there was a very small ferroelectric instability when the lattice was strained to the experimental value. This discrepancy is discussed further at the end of this subsection.

The remaining compounds in this study exhibit transitions in which phonons become soft at points other than Γ in the Brillouin zone. Experimental observations therefore do not preclude the possibility that there may be an unstable Γ point phonon; another transition may simply intervene before the Γ point instability has a chance to freeze in. For example, $SrTiO_3$ is an incipient ferroelectric and by extrapolating the high-temperature form for the dielectric response one would predict a transition to a ferroelectric ground state at 40 K.[1] At atmospheric pressure, however, $SrTiO_3$ makes a transition to a structure with tilted oxygen octahedra at 110 K.

TABLE V. Interaction parameters of eight perovskites in a.u.

	B_{11}	B_{12}	B_{44}	B_{1xx}	B_{1yy}	B_{4yz}	κ	α	γ	α'	γ'
$BaTiO_3$	4.64	1.65	1.84	-2.18	-0.20	-0.08	-0.0175	0.320	-0.473	0.176	-0.124
$SrTiO_3$	5.14	1.38	1.56	-1.41	0.06	-0.11	-0.0009	0.150	-0.191	0.093	-0.010
$CaTiO_3$	5.15	1.22	1.29	-0.59	0.06	-0.10	-0.0115	0.023	-0.006	0.013	0.061
$KNbO_3$	6.54	0.96	1.37	-3.01	0.33	-0.01	-0.0154	0.378	-0.613	0.184	-0.111
$NaNbO_3$	6.63	0.96	1.07	-1.71	0.50	0.00	-0.0124	0.168	-0.256	0.093	-0.041
$PbTiO_3$	4.52	1.97	1.36	-0.78	0.00	-0.03	-0.0129	0.044	-0.045	0.022	0.025
$PbZrO_3$	5.92	1.37	1.07	-0.22	0.07	-0.01	-0.0156	0.011	-0.013	0.009	-0.003
$BaZrO_3$	5.52	1.56	1.47	-0.47	0.07	-0.11	0.0078	0.016	0.000	0.009	0.054

TABLE VI. Summary of the theoretical and experimental ground-state structures of the eight perovskites. Abbreviations are ferroelectric (FE), antiferroelectric (AF), antiferrodistortive (AFD), rhombohedral (R), tetragonal (T), monoclinic (M), cubic (C), and orthorhombic (O).

	Theory	Expt. (primitive)	Expt. (complex)
$BaTiO_3$	FE-R	FE-R	
$SrTiO_3$	FE-R		AFD-T
$CaTiO_3$	FE-T		O
$KNbO_3$	FE-R	FE-R	
$NaNbO_3$	FE-R		FE-M
$PbTiO_3$	FE-T	FE-T	
$PbZrO_3$	FE-R	FE-R[a]	AF-O
$BaZrO_3$	C	C	

[a] Extrapolated from the phase diagram of PZT.

A direct comparison between the theoretical and experimental soft-mode eigenvectors can be made for the cases of $BaTiO_3$, $KNbO_3$, and $PbTiO_3$, using the experimentally measured ionic displacements for the ferroelectric phase.[29–31] The results are summarized in Table VII. In all cases the soft-mode amplitude is underestimated by the fourth-order theory. Typically the error is about 30%. This size and sign of error is not surprising in view of the fact that our calculations underestimate the theoretical lattice constant, and that this and other studied[3,4,6,7] have shown that the soft-mode surface is a sensitive function of volume. For the case of $BaTiO_3$, our results for the soft-mode eigenvector are in good accord with the experimental data, a result we found in our previous work.[3,7] However, the level of agreement is less satisfactory for $KNbO_3$ and still worse for the case of $PbTiO_3$, which has the largest spontaneous distortion. We have tried relaxing the ions in $PbTiO_3$ at the experimental lattice constant and c/a ratio. The displacement vector obtained in this case is (0.73,0.32,−0.36,−0.36,−0.32), which is clearly in much better accord with the experimental data. The soft-mode amplitude was also brought in closer agreement with experiment, coming out to be 0.913 a.u. Thus, we conclude that for the compounds with the largest spontaneous distortion, the fourth-order expansion should not be trusted to describe the energy surface with quantitative accuracy all the way to the distorted equilibrium structure.

The elastic constants for the eight perovskites were computed by examining the behavior of the total energy as a function of strain. Data generated in the previous section were used to compute the bulk modulus by fitting a third-order polynomial through the energy vs lattice constant data. A typical example of the quality of fit is shown in Fig. 1(a) where we show our results for the case of $PbTiO_3$. The two remaining independent elastic constants, which were taken to be B_{11} and B_{44}, were obtained by freezing in strains which lowered the symmetry of the cells to tetragonal or rhombohedral symmetry, and again fitting the energy vs strain curves with a third-order polynomial. At least five different values of the strain were employed to obtain each elastic constant in each material.

The elastic constants we have obtained for the perovskites appear to be in good agreement with previous theoretical results in the few places we have been able to make comparisons. Singh and Boyer[6] found a bulk modulus of 195 GPa in their FLAPW work on $KNbO_3$ which agrees to about 2% with the value of 199 GPa found here. Cohen,[32] also using the FLAPW method, obtained a bulk modulus of 215 GPa for $PbTiO_3$, which is about 3% larger than our value of 209 GPa. The best available experimental elastic constants on the cubic phases of the materials studied here appear to be for $SrTiO_3$.[8] The Landolt-Börnstein tables quote room temperature ranges of 316–348 GPa, 101–103 GPa, and 119–124 GPa for c_{11}, c_{12}, and c_{44}, respectively, which can be compared with our own values of 389 GPa, 105 GPa, and 155 GPa. Overall the level of agreement between theory and experiment is about 20%, which is not as good as one would generally expect from an LDA calculation. However, it must be borne in mind that the cubic phase of $SrTiO_3$ is unstable, and that the measured elastic constants are quite strong functions of temperature. For example according to the results of Bell and Rupprecht[33] c_{11} increases by about 4% as the temperature is lowered from room temperature to −160 °C, before dropping precipitously as the transition temperature is approached. It is therefore unclear whether a direct comparison of the

TABLE VII. Comparison of theoretical and experimental soft-mode amplitudes and vectors. Amplitudes are in bohrs, and vectors are normalized to unity.

	$BaTiO_3$		$KNbO_3$		$PbTiO_3$	
	Theory	Expt.[a]	Theory	Expt.[b]	Theory	Expt.[c]
$\xi_z^A(j_{soft},z)$	0.20	0.22	0.18	0.32	0.57	0.72
$\xi_z^B(j_{soft},z)$	0.76	0.76	0.80	0.73	0.51	0.33
$\xi_z^{O_I}(j_{soft},z)$	-0.21	-0.23	-0.31	-0.33	-0.41	-0.35
$\xi_z^{O_{II}}(j_{soft},z)$	-0.21	-0.23	-0.31	-0.33	-0.41	-0.35
$\xi_z^{O_{III}}(j_{soft},z)$	-0.53	-0.52	-0.37	-0.38	-0.27	-0.35
Amplitude	0.25	0.31	0.22	0.37	0.54	0.82

[a] Ref. 29.
[b] Ref. 30.
[c] Ref. 31.

theoretical and experimental elastic constants for the cubic symmetry structure is valid and in view of these uncertainties we were satisfied with the level of agreement obtained.

The phonon strain interaction parameters B_{1xx}, B_{1yy}, and B_{4yz} were found by freezing in a small amount of the soft-mode vector (typically we used $u = 0.005a$) and computing the changes in the forces on the ions for five different strains. Results for our calculation of B_{1xx} in the case of $PbTiO_3$ are shown in Fig. 1(b). It is apparent from Table V that the most important strain-phonon coupling arises through the term B_{1xx} terms which tend to be large and are always negative. Physically B_{1xx} measures the extent to which the x-polarized soft-mode eigenvalue changes on application of an η_1 strain. The negative sign of this coupling constant is reasonable, because compression of the lattice in the x direction (application of a negative η_1) will tend to increase the ion-ion repulsions and hence raise the soft-mode eigenvalue. In Fig. 2 we plot B_{1xx} as a function of the soft-mode angle. It is apparent that B_{1xx} shows a marked tendency to become more negative as the soft-mode angle decreases. Given that a small soft-mode angle implies large motion of the B cation, this suggests that B_{1xx} is most sensitive to the B-O interactions in the cell, and that the B-O bond stiffens rapidly as it is compressed.

Finally α and γ were obtained by freezing in the soft-mode distortion for a range of values of u in the [100] and [111] directions and fitting the resulting energy vs displacement curves with a quadratic polynomial in the square of the soft-mode coordinate. Typical results for the case of $PbTiO_3$ are illustrated in Fig. 1(c). The resulting sets of parameters are summarized in Table V. The final two columns of this table give the values of α' and γ' as defined in Sec. II.

Perhaps the most successful aspect of Table V is that it correctly predicts the symmetry of the ground-state structures of all the compounds with primitive five-atom unit cells. For clarity we have summarized the theoretical and experimental results in Table VI. γ' is negative for $BaTiO_3$ and $KNbO_3$, and so these materials should have rhombohedral structures as their lowest-temperature structures according to our fourth-order theory. $PbTiO_3$, on the other hand, has a positive value of γ' and is thus correctly predicted to have a tetragonal ground state. A further interesting case is provided by $PbZrO_3$. While pure $PbZrO_3$ has a rather complicated

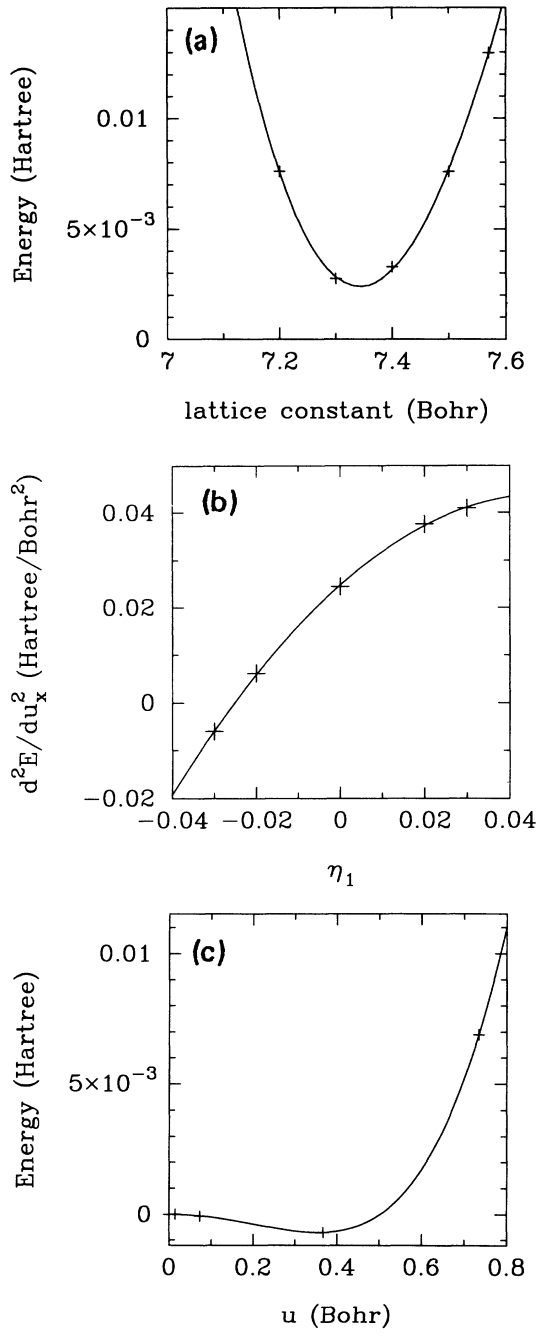

FIG. 1. Sample fits used to obtain interaction parameters of $PbTiO_3$. (a) shows fit of energy vs lattice constant. (b) depicts $\frac{\partial^2 E}{\partial u_x^2}$ as an η_1 strain is frozen into the cell. (c) shows the variation of the energy as the soft-mode amplitude is increased for the case $u_x = u$, $u_y = u_z = 0$.

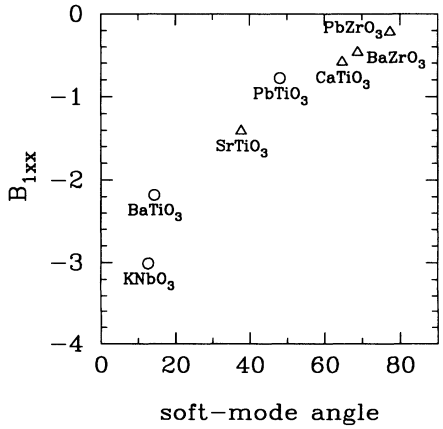

FIG. 2. Strain-phonon interaction parameter B_{1xx} in hartree/bohr^2 against soft-mode angle in degrees.

ground-state structure, it is found that the solid solution $PbTi_xZr_{1-x}O_3$ (PZT) has a simple ferroelectric structure in the range $0.1 < x < 1.0$. The ground-state structure undergoes a transition from a tetragonal to a rhombohedral phase at a composition of x about 0.5 as $PbZrO_3$ is added to $PbTiO_3$.[1] It is therefore also reasonable that γ' should be negative for $PbZrO_3$ as observed in Table V.

We return now to discuss the discrepancy between our results and those of Singh and Boyer.[6] As noted earlier, these authors found that $KNbO_3$ is stable in the cubic structure at the theoretical lattice constant, whereas the current work predicts $\kappa < 0$ and a rhombohedral ground-state structure. The origins of this discrepancy are unclear at this time. Part of the explanation may lie in the higher-quality k-point sets used here, as the trends observable in Table II suggest that incomplete convergence of the Brillouin zone integrations leads to an overestimate of κ. Our experience has been that the calculation of the soft-mode eigenvalue in a ferroelectric is a much more difficult calculation than the apparently similar problem of obtaining the phonon frequencies of a semiconductor such as Si. In the previous section it was demonstrated that this quantity is unusually sensitive to k-point sets and plane-wave cutoff. However, this probably does not account for the whole difference between our results, and we think it is too early to decide whether the present work or that of Singh and Boyer is closer to the "exact LDA" answer. On the one hand, we are clearly in closer agreement with experiment than the FLAPW calculations; on the other hand, it is to be admitted that the pseudopotential method makes an additional approximation over the FLAPW method. This uncertainty highlights the need for further high-quality calculations by other groups using independent codes and methods to more accurately quantify the size of the LDA errors in these materials.

C. Band structures

We have calculated the band structures for each perovskite. In each case we worked with the unit cell with full cubic symmetry at the theoretical lattice constant. Figure 3 shows our results for $PbTiO_3$. The energy scale is in eV, and the origin of energy was arbitrarily set to be at the valence band maximum. A visual comparison of our results for this material against those of Cohen and Krakauer[4] shows almost no discernible difference. In Fig. 4 we show the results of our calculation for all eight materials between Γ and X. In each material there is a fairly narrow set of oxygen $2s$ bands between about -16.0 and -18.0 eV, and a group of oxygen $2p$ states between 0.0 and -5.0 eV. Also visible on this scale is a number of shallow core states associated with the A cation, which we have labeled individually in Fig. 4. It can be seen that these shallow core states have the most influence on the upper valence bands and lower conduction bands in the case of the lead compounds.

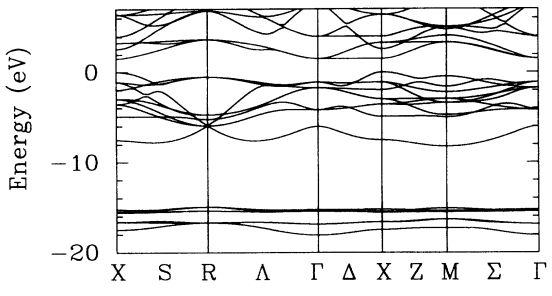

FIG. 3. Band structure of cubic $PbTiO_3$ for selected high-symmetry directions.

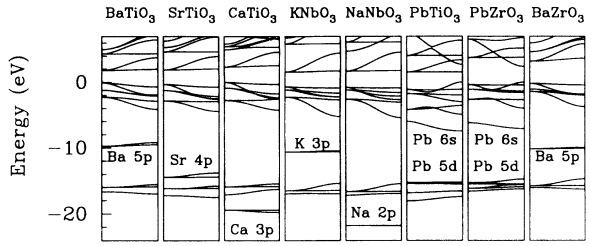

FIG. 4. Comparison of the band structures of eight perovskite compounds in the cubic structure from Γ to X.

Our band-structure calculation for $SrTiO_3$ is also in good agreement with the LAPW calculation of Mattheiss;[34] the small differences that do occur presumably reflect the neglect of relativistic effects in the latter. Our calculations for all eight materials show the same characteristic flatness of certain bands (e.g., the lowest conduction band along Γ to X) as was found by Mattheiss for $SrTiO_3$ and several other cubic perovskites.[34] The fitting of the perovskite band structures to tight-binding models has been discussed by Mattheiss,[34] Harrison,[35] and Wolfram and Ellialtioğlu.[36] The latter authors relate the observed flatness of the bands to certain unusual features in the density of states and optical response which appear to be characteristic of two-dimensional systems.

D. Analysis of structural trends

Here, we discuss whether the results obtained above can be understood on the basis of simple models and chemical trends. As discussed in the previous subsection, it is clear that band-structure features are best discussed in the context of a tight-binding description.[34–36] Here, our emphasis is on structural energetics.

A number of trends in our soft-mode data can be understood in a qualitative way in terms of δ, the parameter introduced in Sec. IV A to reflect the frustration in the ionic radii. Intuitively we might expect that those materials with the values of δ which are closest to zero should be the most stable materials in the cubic perovskite phase and might therefore tend to have the largest values of soft-mode eigenvalue. In Fig. 5 we plot κ in a.u. against δ in a.u. In order to slightly increase the database of results we have also included in the plot values obtained for $SrZrO_3$ and $CaZrO_3$. There does appear to be some tendency for κ to peak around $\delta = 0$. The trend is perhaps most convincing if one focuses on groups of chem-

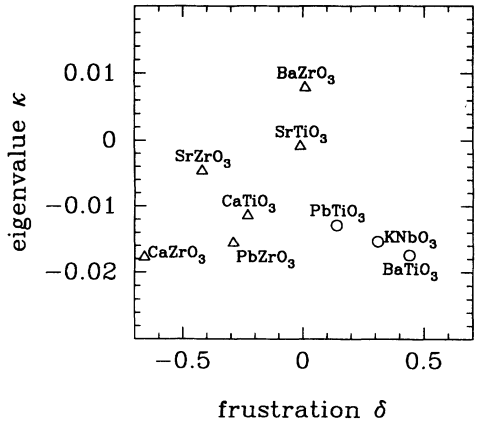

FIG. 5. Soft-mode eigenvalues (hartree/bohr^2) against frustration (bohrs) for nine perovskite compounds. Materials with primitive five-atom ferroelectric ground states are plotted as circles. All other cases are shown as triangles.

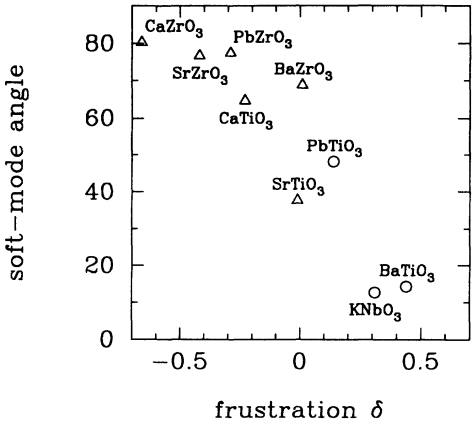

FIG. 6. Soft-mode angle in degrees vs frustration (bohrs). Symbols as in Fig. 5.

ically similar compounds, such as the $BaZrO_3$, $SrZrO_3$, $CaZrO_3$ series where κ decreases steadily as δ decreases from about 0.0 a.u. to about -0.7 a.u., or the $BaTiO_3$, $SrTiO_3$, $CaTiO_3$ series, which is peaked at $SrTiO_3$ with $\delta = -0.01$.

Interestingly, the three compounds with ferroelectric ground states with five atoms in the primitive cell (depicted with circles in Fig. 5) are the compounds with significantly positive values of δ. While we think that the above observations form a useful point of view for analyzing our data, it is important to point out that a simple analysis in terms of our frustration parameter δ has its limitations. For example the compound $KTaO_3$ has exactly the same value of δ as $KNbO_3$ according to the Shannon-Prewitt tables. However $KTaO_3$ is believed to be stable in the cubic perovskite structure at all temperatures.[1,8] Thus we have an example of a material with a substantial positive value of δ which is not ferroelectric and must have $\kappa > 0$.

We have also considered the behavior of the soft-mode eigenvector, $\xi^\tau_\alpha(j_{\rm soft}, \alpha)$ as a function of δ. For positive δ the B ions are likely to be "loose" in their sockets because the A-O interactions expand the lattice beyond the ideal B-O value. It is reasonable to expect that the magnitude of $\xi^B_\alpha(j_s, \alpha)$ will be greater than $\xi^A_\alpha(j_s, \alpha)$ in these circumstances. The converse should hold true for the situation where $\delta < 0$. In Fig. 6 we have plotted the soft-mode angle defined as $\tan^{-1}\left[\xi^A_\alpha(j_s, \alpha)/\xi^B_\alpha(j_s, \alpha)\right]$ in degrees against δ in bohrs. The first point of note is that all the angles are positive, which implies that in all cases the A and B cations move in the same direction in the soft mode. As expected, there is a convincing trend for the A cation motion to decrease with increasing δ.

Of course, δ is a purely "classical" measure of ionic radius. However, the perovskites are only weakly ionic. For example, the hopping $V_{pd\sigma}$ between nearest-neighbor O $2p$ and Ti $3d$ orbitals is found to be on the same order as the energy separation between these levels, about 3 eV.[34] Thus it is clear that p-d hybridization must make a contribution to the crystal cohesion and must play a role in the ferroelectric instabilities. One is therefore led to look for correlations of computed structural properties with chemical trends and isoelectronic relationships. However, such trends are not very evident in Table V. Focusing just on the elastic constants (the only quantities which do not involve the soft mode), one does see that the two compounds of the form I-Va-O_3 ($NaNbO_3$ and $KNbO_3$) have larger values of B_{11} and smaller values of B_{12} than the other six materials. This is most likely due to the difference in Madelung energies. However, a systematic dependence of computed quantities upon the species of the B cation, as might be expected from the role of the latter in hybridizing with the oxygen, is not evident. For example, while $NaNbO_3$ and $KNbO_3$ might be expected to behave similarly on chemical grounds, many of the quantities listed beyond the third column of Table V are quite different. This is because these quantities all depend indirectly upon the soft-mode eigenvector, which is quite different for the two materials (for which the soft-mode angle defined above is 36° and 13° respectively). Thus, despite the expected importance of p-d hybridization, it appears that simple arguments based on ionic radii are surprisingly effective.

V. DISCUSSION

Here, we comment briefly on some of the implications of our results.

We find that the sign of the effective fourth-order coupling is positive in all directions in all eight materials. (As can be seen from Sec. II, this effective fourth-order coupling ranges from α' to $\alpha' + \gamma'/3$, depending on direction; Table V shows that this quantity is always positive, even after renormalization by strain coupling is taken into account.) In the Landau-type theories of the ferroelectric phase transition, the sign of the fourth-order term in the order-parameter expansion of the free energy determines whether the transition is of first or second order.[1] Of course, at $T > 0$ the free energy is renormalized by anharmonic coupling of the soft-mode variable to

other phonons, which is not included in our calculations. Thus, at least for the compounds studied, we conclude that coupling to strain alone is insufficient to drive the fourth-order term negative as required for a first-order transition. In those cases where the transition is observed to be first order, the anharmonic phonon couplings must be responsible.

The bare coupling constant γ is almost always found to be negative in the materials studied here. The strain renormalizations were always found to increase the value of this quantity (i.e., $\gamma' > \gamma$), and in a couple of cases cause it to switch sign. These observations serve to highlight the important consequences of strain coupling in the perovskites, as emphasized previously by Cohen and Krakauer[4] in their study of $PbTiO_3$. Moreover, they provide a possible explanation for a well-known asymmetry in the observed sequences of phase transitions: namely, that those materials like $BaTiO_3$ which are rhombohedral at $T = 0$ typically pass through tetragonal and sometimes orthorhombic phases on the way from the cubic phase, while those materials such as $PbTiO_3$ which are tetragonal at $T = 0$ usually transform directly from the cubic phase. In the former case, the sequence of transitions is usually rationalized in terms of an eight-site model, in which the order parameter just above the transition to the cubic phase is assumed to spend most of its time fluctuating among the eight minima in the $\langle 111 \rangle$ directions. Just below the transition, it freezes onto a subset of four of these minima, with average $\langle 100 \rangle$ orientation and tetragonal symmetry; only at very low temperature does it freeze into a single minimum and acquire rhombohedral symmetry. This scenario requires that the sites along the $\langle 111 \rangle$ directions be minima even in the cubic phase, *before* the strain develops. That is, it requires that γ and γ' be of the same sign (in this case, negative). Insofar as $\gamma' > \gamma$, this is automatic for rhombohedral $T = 0$ materials, which must have $\gamma' < 0$. If both γ and γ' were of positive sign, one might imagine a scenario in which a "six-site model" would give rise to a transition from cubic to rhombohedral, orthorhombic, and tetragonal, as the order parameter freezes onto subsets of three, two, and one $\langle 111 \rangle$ minima, respectively. However, for $PbTiO_3$ we have γ and γ' of opposite sign, so that such a scenario is not plausible. If this situation is typical of materials with tetragonal $T = 0$ structures, it would explain why the reversed sequence is not observed.

We emphasize that we do not have in hand all the elements needed to construct a theory of the phase transition from first principles. Nevertheless, we have obtained many of the ingredients that would enter such a theory.[9] In particular, we have calculated virtually all the relevant *on-site* couplings, including anharmonic and strain couplings. The most pressing need now is for calculations which will determine some of the *intercell* couplings, especially those at harmonic order. These can be extracted from LDA calculations for phonons away from the Brillouin zone center, using either the supercell frozen phonon approach or a linear response approach. Thus it appears that it may not be long before a thermodynamic theory of the phase transitions in perovskite ferroelectrics may be constructed from first principles.

Of course, the results presented here remind us of a serious limitation of the first-principles LDA approach, connected with the extreme sensitivity of some calculated quantities to the lattice constant. As discussed in the body of the paper, we find that LDA underestimates lattice constants by approximately 1% in perovskites, as is common for other materials. Unfortunately, because of the proximity to the ferroelectric phase transition in the perovskites, this 1% error can translate into large errors in such quantities as the magnitude of the $T = 0$ distortion, the spontaneous polarization, and ultimately, in the ferroelectric transition temperature. However, there is no reason to expect it to have a radical effect on many of the other calculated quantities, such as the values of the anharmonic and strain couplings and the soft-mode eigenvectors. If and when it becomes possible to calculate pressure-temperature phase diagrams from first-principles LDA calculations, we anticipate that the pressure axis may have to be artificially shifted to accommodate the $\sim$1% lattice-constant error. But we are optimistic that the structure of the phase diagram (sequence of phases, first-order vs second-order transitions, boundaries, etc.) will otherwise be reliable.

VI. CONCLUSIONS

We have performed accurate first-principles pseudopotential calculations on eight perovskite compounds within an ultrasoft-pseudopotential approach and the LDA. We have shown that it is possible to devise a computationally tractable scheme to compute the soft-mode total-energy surface correct to fourth order in the soft-mode displacement. Our convergence tests highlight the need for extreme accuracy in the k-point sets in these calculations.

We find that zone-center instabilities in the cubic perovskite structure are very common, and that all the compounds studied here which have an experimental phase transition also have a zone-center soft mode at the theoretical LDA lattice constant, even in cases where the observed transitions are caused by soft modes away from the Γ point. We find that the LDA correctly predicts the symmetry of the ground-state structures of $BaZrO_3$, $BaTiO_3$, $KNbO_3$, and $PbTiO_3$. The remaining compounds have ground-state unit cells with more than five atoms, and the determination of their ground states therefore lies beyond the scope of the present study.

ACKNOWLEDGMENTS

We would like to thank Doug Allan, James Annett, Ron Cohen, Karin Rabe, and Mike Teter for illuminating discussions on various aspects of the methods and calculations in this paper and Ron Cohen and David Singh for making unpublished FLAPW results available to us. This work was supported by the Office of Naval Research under Contract No. N00014-91-J-1184.

APPENDIX A

Our objective here is to solve the matrix equation for the strain $\tilde{\eta}_i$ which minimizes the total energy for a given set of u_α. The symmetry of the problem becomes most readily apparent if we define a new vector y_i with components $y_1 = u_x^2$, $y_2 = u_y^2$, $y_3 = u_z^2$, $y_4 = u_y u_z$, $y_5 = u_z u_x$, $y_6 = u_x u_y$. With this notation Eq. (14) can be written as

$$0 = \sum_i B_{ij}\tilde{\eta}_j + \frac{1}{2}\sum_j C_{ij} y_j \ , \tag{A1}$$

where $\mathbf{B}$ and $\mathbf{C}$ are both 6×6 matrices with the structure

$$\mathbf{M} = \begin{bmatrix} P & Q & Q & 0 & 0 & 0 \\ Q & P & Q & 0 & 0 & 0 \\ Q & Q & P & 0 & 0 & 0 \\ 0 & 0 & 0 & R & 0 & 0 \\ 0 & 0 & 0 & 0 & R & 0 \\ 0 & 0 & 0 & 0 & 0 & R \end{bmatrix} . \tag{A2}$$

For the $\mathbf{B}$ matrix $P = B_{11}$, $Q = B_{12}$, and $R = B_{44}$, while for $\mathbf{C}$ we have $P = B_{1xx}$, $Q = B_{1yy}$, and $R = 2B_{4yz}$. Because $\mathbf{M}$ is a symmetric matrix it can be written as

$$\mathbf{M} = \mathbf{Z}\mathbf{\Lambda}(\mathbf{M})\mathbf{Z}^\dagger, \tag{A3}$$

where $\mathbf{\Lambda}(\mathbf{M})$ is the diagonal matrix of eigenvalues of $\mathbf{M}$ and $\mathbf{Z}$ is the matrix of orthonormal eigenvectors. The eigenvalues are just $P + 2Q$ (1), $P - Q$ (2), and R (3), where the number in parentheses gives the degeneracy. In terms of the bulk and shear moduli defined in Eqs. (17a)–(17f) the eigenvalues of $\mathbf{B}$ are B, $2\mu_t$, and μ_r, while the eigenvalues of $\mathbf{C}$ are C, $2\nu_t$, and $2\nu_r$. The eigenvectors of a matrix of the form $\mathbf{M}$ can be chosen to be independent of the values of P, Q, and R. For example one simple choice is

$$\mathbf{Z} = \begin{bmatrix} \frac{1}{\sqrt{3}} & 0 & -\frac{2}{\sqrt{6}} & 0 & 0 & 0 \\ \frac{1}{\sqrt{3}} & \frac{1}{\sqrt{2}} & \frac{1}{\sqrt{6}} & 0 & 0 & 0 \\ \frac{1}{\sqrt{3}} & -\frac{1}{\sqrt{2}} & \frac{1}{\sqrt{6}} & 0 & 0 & 0 \\ 0 & 0 & 0 & 1 & 0 & 0 \\ 0 & 0 & 0 & 0 & 1 & 0 \\ 0 & 0 & 0 & 0 & 0 & 1 \end{bmatrix} . \tag{A4}$$

It is clear that the expression for $\tilde{E}$ given in Eq. (15) can be written as

$$\tilde{E}(\{u_\alpha\}) = E^{(0)} + \Phi(\{u_\alpha\}) - \frac{1}{8}\sum_{ij} y_i \left[\mathbf{Z}\mathbf{\Lambda}(\mathbf{C})\mathbf{Z}^\dagger\mathbf{Z}\mathbf{\Lambda}^{-1}(\mathbf{B})\mathbf{Z}^\dagger\mathbf{Z}\mathbf{\Lambda}(\mathbf{C})\mathbf{Z}^\dagger\right]_{ij} y_j . \tag{A5}$$

For a symmetric matrix we have $\mathbf{Z}^\dagger\mathbf{Z} = \mathbf{1}$ and thus it is obvious that the matrix in square brackets is just another matrix of the form $\mathbf{M}$ with eigenvalues $\frac{C^2}{B}$, $2\frac{\nu_t^2}{\mu_t}$, and $4\frac{\nu_r^2}{\mu_r}$. Given the relationship between the eigenvalues and P, Q, and R the components of this matrix are just

$$P = \frac{1}{3}\left(\frac{C^2}{B} + 4\frac{\nu_t^2}{\mu_t}\right), \tag{A6a}$$

$$Q = \frac{1}{3}\left(\frac{C^2}{B} - 2\frac{\nu_t^2}{\mu_t}\right), \tag{A6b}$$

and

$$R = 4\frac{\nu_r^2}{\mu_r}. \tag{A6c}$$

It is now simply a matter of multiplying out the matrix term in Eq. (A5) and using the definition of y_i in terms of u_α to derive Eq. (16).

APPENDIX B

In this appendix we describe the conjugate-gradient (CG) scheme which was employed in the calculations presented in this paper to minimize the Kohn-Sham functional. Probably the best known CG method for use in fast Fourier transform (FFT) based pseudopotential codes is that due to Teter, Payne, and Allan[37] which has been applied with great success to a wide range of problems. This method minimizes the total energy in a band-by-band fashion. Orthogonality is maintained by projecting out from the conjugate direction $\mathbf{h}$ all components of the vector which are parallel to orbitals at the current k point. The algorithm is further improved with preconditioning based on the diagonal dominance of the kinetic energy at large reciprocal lattice vectors. Teter *et al.* have emphasized the importance of updating the Kohn-Sham Hamiltonian self-consistently on each iteration in order to control the "charge sloshing" instabilities caused by the divergent behavior of the Coulomb interaction at long wavelengths.

We have chosen to formulate our CG scheme using a generalization of the Kohn-Sham energy functional to nonorthogonal orbitals in a manner which is very similar to an idea which was recently proposed by Galli and Parrinello.[38] Two major benefits arise from this general functional. First, the CG algorithm does not lend itself easily to constrained minimization problems, particularly if one should wish to move away from band-by-band types of schemes. By choosing to work with nonorthogonal orbitals, we dispense with the need to impose the orthogonality constraint during the course of the minimization process. Second, the nonlocal overlap operator $\hat{S}$ which occurs in the Vanderbilt ultrasoft-pseudopotential scheme is easily incorporated into the formalism.

A second major ingredient of our method is to minimize the Kohn-Sham functional with respect to all the wave-function degrees of freedom simultaneously. In the one-band-at-a-time approach it is fruitless to iterate any

given band to self-consistency, because iterating on later bands changes the total potential, destroying the self-consistency of previous bands. The sequential approach limits the number of CG steps which can usefully be performed on any given band to about 5.[37] Within the approach preferred here, where all bands at all k points are changed on each iteration, this self-consistency consideration does not come into play and as many CG steps as desired can be performed before a restart. Our experience has been that one set of 20 steps of the CG algorithm is considerably more efficient that four sets of 5 steps and that quite substantial gains in performance can therefore be made.

In the following we shall develop our formulation for the case where the number of electrons in each occupied band at each k point is the same. This restriction is not necessary and the question of how to handle the more general case of variable occupation has recently been addressed by Arias *et al.*[39] We shall also concentrate on the case where we have a single k point, as the extension to the multiple k-point case is trivial. Within the ultrasoft framework the Kohn-Sham functional is written in terms of a set of linearly independent nonorthogonal orbitals $\{\phi_i\}$ as

$$E_{\rm tot}[\{\phi_i\},\{\mathbf{R}_I\}] = \sum_i \langle\phi_i \mid -\tfrac{1}{2}\nabla^2 + V_{\rm NL} \mid \overline{\phi}_i\rangle + \frac{1}{2}\int\int d\mathbf{r}d\mathbf{r}' \frac{n(\mathbf{r})n(\mathbf{r}')}{\mid \mathbf{r}-\mathbf{r}' \mid} + E_{\rm xc}[n] + \int d\mathbf{r} V_{\rm loc}^{\rm ion}(\mathbf{r})n(\mathbf{r}) + U(\{\mathbf{R}_I\}), \tag{B1a}$$

where the charge density $n(\mathbf{r})$ is given by

$$n(\mathbf{r}) = \sum_i \phi_i^*(\mathbf{r})\overline{\phi}_i(\mathbf{r}) + \sum_i \sum_{nmI} Q_{nm}^I(\mathbf{r})\langle\phi_i \mid \beta_m^I\rangle\langle\beta_n^I \mid \overline{\phi}_i\rangle, \tag{B1b}$$

with

$$\overline{\phi}_i = \sum_j \phi_j T_{ji} \tag{B1c}$$

and

$$\left[T^{-1}\right]_{ji} = \langle\phi_j \mid \hat{S} \mid \phi_i\rangle. \tag{B1d}$$

In Eq. (B1a) $V_{\rm NL}$ is the nonlocal potential, $V_{\rm loc}^{\rm ion}$ is the local ionic potential, i is an index running over all occupied bands, n and m are indices running over projector functions $\mid\beta\rangle$ on a given atom, I is an index running over atoms, and $U(\{\mathbf{R}_I\})$ is the ion-ion interaction energy. A complete discussion of all of the meaning of the terms in Eq. (B1a) can be found in Ref. 14. Conventionally the Kohn-Sham energy in the Vanderbilt scheme is written in terms of a set of $\hat{S}$-orthonormal orbitals.[14] The energy computed in Eq. (B1a) is identical to that computed with the conventional expression using any set of of $\hat{S}$-orthonormal orbitals which span the same space as $\{\phi_i(\mathbf{r})\}$. Note that the above expressions are equally applicable to the more usual plane-wave formulations using Kleinman-Bylander potentials: This limit is recovered by setting $\hat{S}$ to the unit operator and the $Q_{nm}^I(\mathbf{r})$ functions to zero.

The functional derivative of $E_{\rm tot}$ with respect to ϕ_i^* (Ref. 38) is given by

$$\frac{\delta E_{\rm tot}}{\delta\phi_i^*} = \hat{H} \mid \overline{\phi}_i\rangle - \sum_j \hat{S} \mid \overline{\phi}_j\rangle\langle\phi_j \mid \hat{H} \mid \overline{\phi}_i\rangle, \tag{B2}$$

where $\hat{H}$ is the usual Kohn-Sham Hamiltonian in the Vanderbilt ultrasoft scheme.[14] Note that since $\langle\phi_k \mid \hat{S} \mid \overline{\phi}_j\rangle = \delta_{kj}$ we have $\langle\phi_k \mid \frac{\delta E_{\rm tot}}{\delta\phi_i^*}\rangle = 0$, which implies that the projection of any occupied orbital on the gradient direction is zero. Physically, adding any amount of the state ϕ_k to the state ϕ_i does not change the subspace spanned by the occupied orbitals and thus leaves the total energy unchanged.

We start our CG iteration with a set of $\hat{S}$-orthonormal $\{\phi_i\}$ obtained from a random number generator or a previous calculation and compute a G-space diagonal preconditioning matrix $\mathbf{K}$ following the algorithm of Teter *et al.*[37] A standard preconditioned CG algorithm is then used to minimize the Kohn-Sham functional. Thus on iteration $n+1$ our gradient is just

$$\mathbf{g}^{n+1} = -\frac{\delta E_{\rm tot}^n}{\delta\phi_i^*}\ , \tag{B3a}$$

where it is implicit that the gradient is to be evaluated with the orbitals $\{\phi_i^n\}$ obtained from the nth iteration. The conjugate search direction $\mathbf{h}^{n+1}$ is

$$\mathbf{h}^{n+1} = \mathbf{K}\cdot\mathbf{g}^{n+1} + \gamma^n\mathbf{h}^n\ , \tag{B3b}$$

where

$$\gamma^n = \frac{(\mathbf{g}^{n+1})^\dagger\cdot\mathbf{K}\cdot\mathbf{g}^{n+1}}{(\mathbf{g}^n)^\dagger\cdot\mathbf{K}\cdot\mathbf{g}^n}\ . \tag{B3c}$$

The line minimizations along the conjugate directions are performed using a variant of the method suggested in Ref. 37. We assume that the energy functional varies quadratically in the region of interest. The total energy and gradient at the point in function space $\{\phi_i^n\}$ are known which fixes two parameters of our quadratic form. The final parameter is obtained by taking a small step along the direction $\mathbf{h}^{n+1}$ and recomputing the self-consistent total energy. Typically the size of the trial step is simply taken to be about the size of step which minimized the function on the previous step.

In order to illustrate the benefits of iterating on all the degrees of freedom at once we have performed two calculations on a five-atom unit cell of $BaTiO_3$ using ten k points in the irreducible wedge of the zone. The first calculation proceeded by minimizing one k point at a time using five CG steps at each k point, where as the second calculation iterated on all k points at once and used 15 CG steps between restarts. The results are illustrated in Fig. 7. Each pass through all the bands was counted as five iterations in the k-point-by-k-point case so comparisons could be made. Relaxing all degrees of freedom at once speeds the calculation by about a factor of 2.

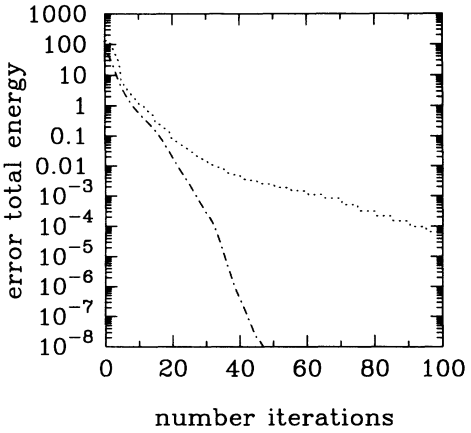

FIG. 7. Error in total energy per unit cell in hartrees vs iteration number using the k-point-by-k-point method (dotted line) and all-k-points-together approach (dashed line).

The operation count per band per iteration is better for a method which updates all the wave-function coefficients together because the Hartree and exchange correlation potential need to be updated much less frequently. This is of particular importance in the Vanderbilt ultrasoft scheme, because augmentation of the density would become a major cost of the calculation if it were done on a band-by-band basis. When all the bands are updated simultaneously the augmentation overhead in the ten k-point calculation discussed above took less than 2% of the time on each CG step. For the size of unit cell considered in this paper the most efficient scheme that we have found for computing the regular contribution to the charge density is to explicitly construct an $\hat{S}$-orthonormal set of orbitals $\{\psi_i\}$ in reciprocal space which span the space of $\{\phi_i\}$. Thus we evaluate $\sum_i \phi_i^*(\mathbf{r})\overline{\phi}_i(\mathbf{r})$ in Eq. (B1b) as $\sum_i \psi_i^*(\mathbf{r})\psi_i(\mathbf{r})$, which can be done with a single FFT per band.

The major drawback of this scheme is that the amount of gradient and conjugate-gradient direction information which must be stored is substantially increased. However, we have found that it is possible to structure the codes so this information is read and written to a disk, without incurring substantial input-output penalties, both on workstations and on the Cray YMP (where we utilized a solid-state disk). In our current implementation of the scheme we use one major work array dimensioned to all the wave functions at all k points and a second smaller array which is sufficient to hold the wave functions at a single k point. Three disk scratch files were used to store current values of $\{\phi_i\}$, the gradient direction, and the conjugate direction.

*Permanent address: Biosym Technologies Inc., 9685 Scranton Rd., San Diego, CA 92122.

[1] M.E. Lines and A.M. Glass, *Principles and Applications of Ferroelectrics and Related Materials* (Clarendon Press, Oxford, 1977).

[2] K.M. Rabe and J.D. Joannopoulos, Phys. Rev. Lett. **59**, 570 (1987); Phys. Rev. B **36**, 6631 (1987).

[3] R.E. Cohen and H. Krakauer, Phys. Rev. B **42**, 6416 (1990).

[4] R.E. Cohen and H. Krakauer, Ferroelectrics **136**, 65 (1992).

[5] R.E. Cohen, Nature **358**, 136 (1992).

[6] D.J. Singh and L.L. Boyer, Ferroelectrics **136**, 95 (1992).

[7] R.D. King-Smith and D. Vanderbilt, Ferroelectrics **136**, 85 (1992).

[8] T. Mitsui *et al.*, *Ferro- and Antiferroelectric Substances*, Landolt-Börnstein, Group III, Vol. 3, edited by K.-H. Hellwege and A.M. Hellwege (Springer-Verlag, Berlin, 1969).

[9] E. Pytte, Phys. Rev. B **5**, 3758 (1972).

[10] D. Vanderbilt, S.H. Taole, and S. Narasimhan, Phys. Rev. B **40**, 5657 (1989).

[11] It is straightforward to show that to lowest order in u_α, $\widetilde{u}_\alpha^j(\{u_\alpha\})$ is given by solution of $\lambda(j)\widetilde{u}_\alpha^j(\{u_\alpha\}) + \frac{1}{6}\sum_{\beta,\gamma,\delta}\left(\partial^4 E/\partial u_\alpha^j \partial u_\beta \partial u_\gamma \partial u_\delta\right)\big|_0 u_\beta u_\gamma u_\delta = 0$. We thus conclude that the variation of $\widetilde{u}_\alpha^j(\{u_\alpha\})$ is at least third order in u_α, and that couplings of the soft mode to other phonons gives rise to sixth-order corrections in the energy.

[12] D. Vanderbilt, Phys. Rev. B **41**, 7892 (1990).

[13] K. Laasonen, R. Car, C. Lee, and D. Vanderbilt, Phys. Rev. B **43**, 6796 (1991).

[14] K. Laasonen, A. Pasquarello, R. Car, C. Lee, and D. Vanderbilt, Phys. Rev. B **47**, 10 142 (1993).

[15] C. Lee, D. Vanderbilt, K. Laasonen, R. Car, and M. Parrinello, Phys. Rev. Lett. **69**, 462 (1992).

[16] A. Pasquarello, K. Laasonen, R. Car, C. Lee, and D. Vanderbilt, Phys. Rev. Lett. **69**, 1982 (1992).

[17] A.M. Rappe, K.M. Rabe, E. Kaxiras, and J.D. Joannopoulos, Phys. Rev. B **41**, 1227 (1990).

[18] L. Kleinman and D.M. Bylander, Phys. Rev. Lett. **48**, 1425 (1982).

[19] D.R. Hamann, M. Schlüter, and C. Chiang, Phys. Rev. Lett. **43**, 1494 (1979).

[20] M.P. Teter, Phys. Rev. B **48**, 5031 (1993).

[21] K. Kunc, R. Zeyher, A.I. Liechtenstein, M. Methfessel, and O.K. Andersen, Solid State Commun. **80**, 325 (1991).

[22] G.B. Bachelet, D.R. Hamann, and M. Schlüter, Phys. Rev. B **26**, 4199 (1982).

[23] D.D. Koelling and B.N. Harmon, J. Phys. C **10**, 3107 (1977).

[24] L. Kleinman, Phys. Rev. B **21**, 2630 (1980).

[25] H.J. Monkhorst and J.D. Pack, Phys. Rev. B **13**, 5188 (1976).

[26] D.M. Ceperley and B.J. Alder, Phys. Rev. Lett. **45**, 566 (1980).

[27] R.D. Shannon and C.T. Prewitt, Acta Crystallogr. B **25**, 925 (1969).

[28] J.C. Slater, Phys. Rev. **78**, 748 (1950).

[29] A.W. Hewat, Ferroelectrics **6**, 215 (1974).

[30] A.W. Hewat, J. Phys. C **6**, 2559 (1973).

[31] G. Shirane, R. Pepinsky, and B.C. Frazer, Acta Crystallogr. **9**, 131 (1955).

[32] R.E. Cohen (private communication).

[33] R.O. Bell and G. Rupprecht, Phys. Rev. **129**, 90 (1963).

[34] L.F. Mattheiss, Phys. Rev. B **6**, 4718 (1972).

[35] W.A. Harrison, *Electronic Structure and the Properties of Solids* (Dover, New York, 1989), Chap. 19.

[36] Ş. Ellialtioğlu and T. Wolfram, Phys. Rev. B **15**, 5909 (1977); T. Wolfram and Ş. Ellialtioğlu, *ibid.* **25**, 2697

(1981).
[37]M.P. Teter, M.C. Payne, and D.C. Allen, Phys. Rev. B **40**, 12 225 (1989).
[38]G. Galli and M. Parrinello, Phys. Rev. Lett. **69**, 3547 (1992).
[39]T.A. Arias, M.C. Payne, and J.D. Joannopoulos, Phys. Rev. Lett. **69**, 1077 (1992).